8

SAR/ISAR Digital Imagery

Chapters 6 and 7 showed that, using either a step-chirp waveform or a deramped/deskewed LFM waveform, we can obtain in wavenumber space (**k**-space) a series of complex samples of radar echoes corresponding to variations in $|\mathbf{k}|$ and $\hat{\mathbf{k}}$ (magnitude and direction of **k**) and that, through the PFA, the RMA, or other focusing procedure, we can transform those data into a form such that performing a weighted FT produces an image of the target area. This chapter investigates more carefully this step of image formation from digitized focused **k**-space data and discusses techniques for obtaining imagery with improved resolution and reduced sidelobes compared with imagery obtained simply using the weighted FT.

We also introduce two other definitions [1]:

- Signal processing, which is the processing of the **k**-space signal to form an image;
- Image processing, which is additional processing performed on the image to improve the contrast, resolution, and so on.

8.1 Digital Image Formation (Signal Processing)

We now investigate the production of a discrete image by means of discrete signal processing.

8.1.1 Real and Complex Imagery

As the received signal enters the antenna, it is characterized by its electric field vector $E(t)$, a sinusoid possessing both amplitude and phase. Its power is

proportional to E^2 (Section 1.3). As the signal passes through the LNA and associated electronics (Section 2.2), and is digitized by the A/D converter, the signal is characterized by a complex voltage with both amplitude and phase, and the power is proportional to the square of the magnitude of the voltage. When the image is formed by FT processing, it is characterized by a (usually two-dimensional) set of pixels, each possessing an amplitude V and phase ϕ. We refer to that as a complex image. When we display a SAR/ISAR image, we usually are interested only in the pixel magnitude. We can display $V(x, y)$, which we shall refer to as a voltage image.

It is often more useful to store or display a SAR/ISAR image using $V^2(x, y)$, which we call the power image (this was assumed in Section 7.3.1). In the signal domain, the power of the recorded signal is proportional to the square of its voltage. In the image domain, we again say that the power of the image pixel is proportional to the square of the magnitude of its voltage, even though the term *energy* might be more appropriate for describing the recorded value of the V^2 of a pixel. Whenever a SAR/ISAR image is displayed, it should be made clear whether the display shows the voltage image or the power image. An advantage of the power image is that Parseval's theorem [2, p. 23] applies: With the proper multiplicative normalization constant (independent of image content), the sum of V^2 (~ energy) in the signal domain equals the sum of V^2 in the image domain. Often the phase is discarded, because only V or V^2 is necessary for ordinary image display; such an image is often referred to as a real image. However, throughout this chapter, the term *image* is used to mean the complex image.

From Sections 6.4 and 7.3.1, we recall that the SAR/ISAR image of a point target is referred to as a PSF or IPR function, characterized by a mainlobe and sidelobes. For uniform weighting (i.e., no weighting), the voltage-image PSF is a sinc function, and the power-image PSF is a sinc-squared function with peak-to-first-null values of

$$\text{Range: } \delta_{rpn} = \frac{c}{2B} \tag{8.1}$$

$$\text{Cross-range: } \delta_{crpn} = \frac{\lambda}{2\Delta\theta} \; (\Delta\theta << 2\pi) \tag{8.2}$$

We refer to those collectively as δ_{pn}. Furthermore, the 3-dB mainlobe width of the sinc-squared function is $(0.886)\delta_{pn}$, and the first sidelobe is 13.3 dB below the mainlobe peak. When a weighting function is applied (Section 6.3.1), the mainlobe is broadened and the sidelobes are lowered relative to the sinc-squared function.

8.1.2 Discrete Fourier Transform

Section 2.1 introduced the continuous FT: The functions in both signal and image domain are defined over a continuous variable. Chapters 2 to 7 referred to the FT without specifying whether it was continuous or discrete. Modern radars generally collect and process a finite set of data samples (digital technology). It is therefore most appropriate to use the discrete FT (DFT), which can be calculated using the highly efficient FFT algorithm. The DFT and its inverse (IDFT) are given by [2, p. 97, using notation therein]:

$$\text{DFT:} \quad G\left(\frac{n}{NT}\right) = \sum_{k=0}^{N-1} g(kT)e^{-j2\pi nk/N} \tag{8.3a}$$

$$\text{IDFT:} \quad g(kT) = \frac{1}{N}\sum_{n=0}^{N-1} G\left(\frac{n}{NT}\right)e^{j2\pi nk/N} \tag{8.3b}$$

Equations (8.3a) and (8.3b) are the discrete form of (2.1). The notation reflects the assumption of time and frequency domains:

- N = number of samples processed (assumed to be sampled uniformly in each domain).
- $k = 0, 1, \ldots, N-1$ = index identifying time-domain sample.
- T = time interval between samples (overall time interval $\approx NT$).
- $g(kT)$ = discrete function in time domain.
- $n = 0, 1, \ldots, N-1$ = index identifying frequency-domain sample.
- $G(n/NT)$ = discrete function in frequency domain (overall frequency interval $\cong 1/T$ for $N >> 1$).

The FFT requires much less computation time than a direct calculation of the DFT. If N is a power of 2, then direct calculation requires N^2 complex multiplications, whereas an FFT of the same N requires only $N(\log_2 N)/2$ complex multiplications [2, pp. 134–135]. For example, if $N = 2^{10} = 1{,}024$, then the FFT requires less than 1/200 the computation time of the direct calculation.

8.1.3 Zero Padding

We often want to sample the frequency-domain function more finely, to see its structure more clearly. A simple way to accomplish that is to use zero-padding. When M zeroes are added to the N time-domain samples, the

frequency-domain function will be sampled at $M + N$ locations over the same interval $1/T$. No information is added. The frequency-domain function will have the same general shape, but it will be sampled more finely and will appear smoother. Figures 8.1, 8.2, and 8.3 illustrate examples of zero-padding using Mathcad®, a software package manufactured by MathSoft, Inc., Cambridge, Massachusetts. The reader can easily verify the procedure with a computer (Problem 8.1). Zero padding is often performed in SAR/ISAR signal processing to produce more finely sampled images.

8.1.4 Formation of a Digital SAR/ISAR Image

From Section 6.3, we have

$$E(\mathbf{k}) \sim \int d\,\mathbf{r}\rho(\mathbf{r})e^{-2j\mathbf{k}\cdot\mathbf{r}} \tag{8.4a}$$

$$\rho(\mathbf{r}) \sim \int d\,\mathbf{k}E(\mathbf{k})e^{2j\mathbf{k}\cdot\mathbf{r}} \tag{8.4b}$$

where $E(\mathbf{k})$ is the complex returned electric field associated with wavenumber $\mathbf{k}$ and $\rho(\mathbf{r})$ is the three-dimensional image. It is convenient to write (8.4) in terms of Cartesian coordinates, because the kernels (the exponential factors) are separable:

$$E(k_x, k_y, k_z) \sim \int e^{-2jk_x x}\int e^{-2jk_y y}\int e^{-2jk_z z}\rho(x, y, z)dxdydz \tag{8.5a}$$

$$\rho(x, y, z) \sim \int e^{2jk_x x}\int e^{2jk_y y}\int e^{2jk_z z}E(k_x, k_y, k_z)dk_x dk_y dk_z \tag{8.5b}$$

Here (x, y, z) are target-centered coordinates, which are fixed relative to the target structure and rotate with the target. Thus, even for constant k, for a rotating target k_x, k_y, k_z will vary.

Equations (8.5a) and (8.5b) were written under the assumption that a continuum (infinite number) of frequencies is transmitted over a continuum of target rotation angles. In reality, the frequencies and angles make up a discrete set rather than a continuum. Thus, after polar-formatting and interpolation, the continuously variable vectors $\mathbf{k}$ and $\mathbf{r}$ are replaced by the discrete sets $(u, v, w)\Delta k$ and $(U, V, W)\Delta r$, where u, v, w, U, V, W are integers. We also assume that the target consists of a discrete set of scatterers, each with voltage reflectivity, q_i, proportional to the square root of its radar cross-section. For this discrete case, (8.5a) and (8.5b) become

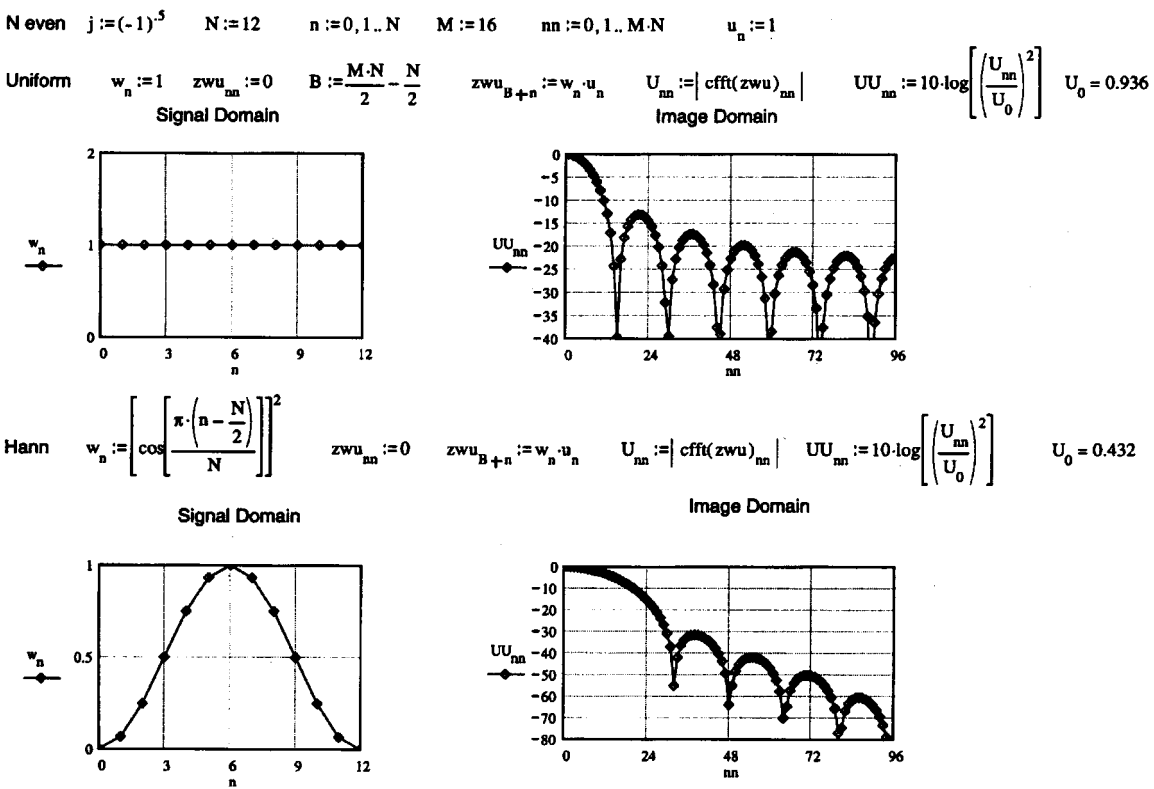

Figure 8.1 Zero-padding procedure.

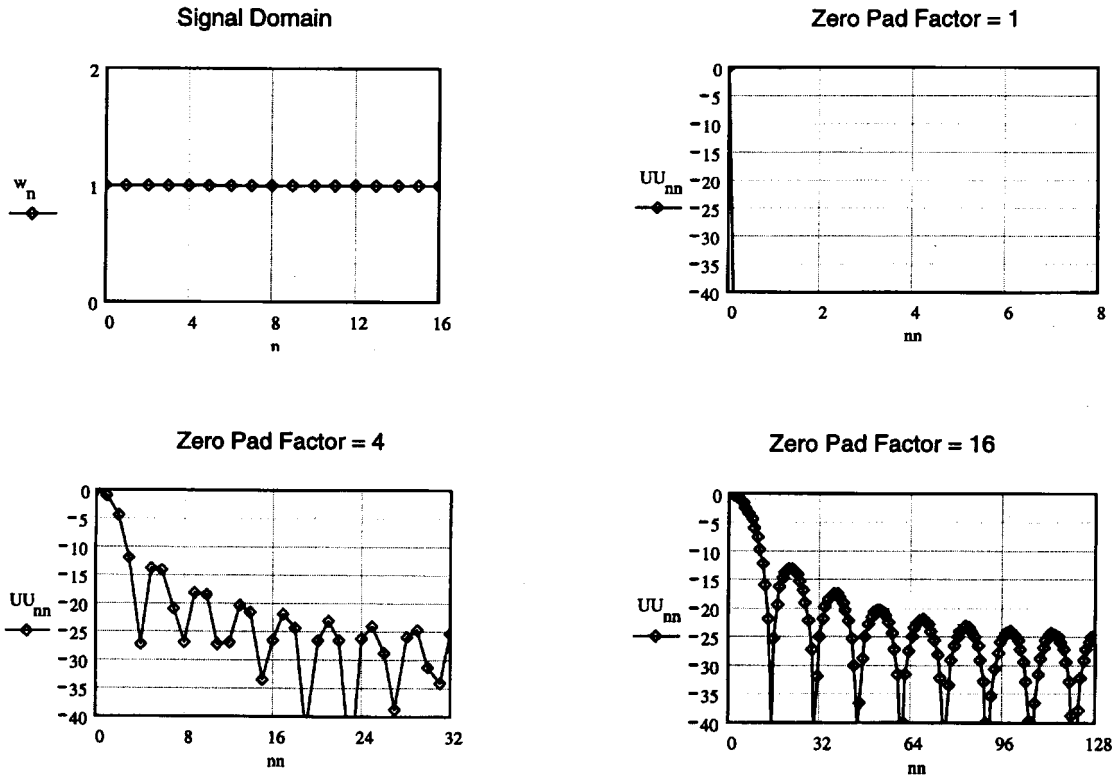

Figure 8.2 Zero-padding, uniform weighting.

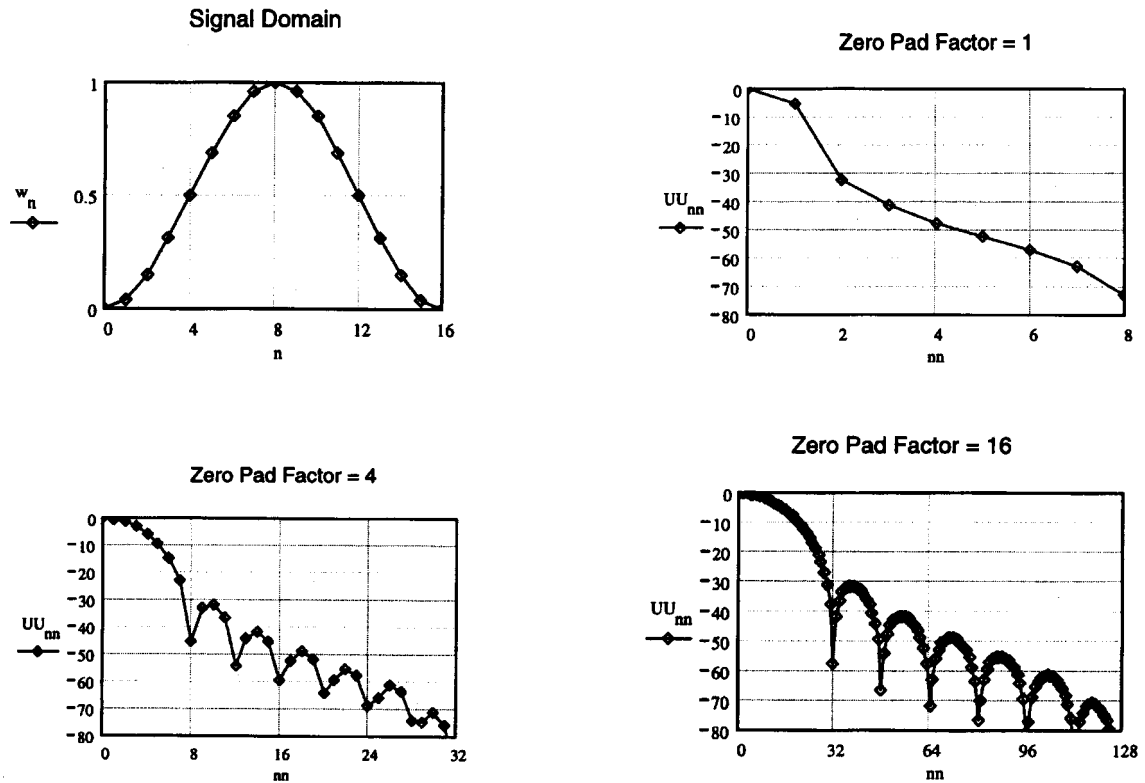

Figure 8.3 Zero-padding, Hann weighting.

$$\text{Signal: } E_{uvw} \sim \sum_i q_i e^{-2j\Delta k(ux_i + vy_i + wz_i)} \tag{8.6}$$

$$\text{Image: } h(U, V, W) = \sum_{u,v,w} E_{uvw} e^{2j\Delta k \Delta r(uU + vV + wW)} \tag{8.7}$$

$$= \sum_i q_i \sum_u e^{-2ju\Delta k(x_i - U\Delta r)} \sum_v e^{-2jv\Delta k(y_i - V\Delta r)} \sum_w e^{-2jw\Delta k(z_i - W\Delta r)} \tag{8.8}$$

(we suppress the normalization constants). (8.8) of a three-dimensional far-field image is a complex function of three space dimensions.

It can be readily shown that the signal history (8.6) can be reconstructed from the image (8.8) (Problem 8.2).

8.1.5 Point-Spread Function

Of particular interest is the PSF, the image resulting from a target consisting of a single point scatter. We let q for the scatterer = 1 and consider only the downrange cut of the PSF. Thus,

$$h_1(U, x) = \sum_{u=u_1}^{u_2} e^{-2ju\Delta k(x - U\Delta r)} \tag{8.9}$$

Here x is the scatterer location (continuous), U is the pixel location (discrete), and u_1 and u_2 are integers. We let $u_2 - u_1 = N - 1$, so there are N values of u. Thus,

$$h_1(U, x) = e^{-2j\Delta k u_1 (x - U\Delta r)} \sum_{u=0}^{N-1} e^{-2j\Delta k u(x - U\Delta r)} \tag{8.10}$$

From Section 2.4.1, we recall

$$\sum_{n=0}^{N-1} e^{jn\psi} = e^{j(N-1)\psi/2} \frac{\sin(N\psi/2)}{\sin(\psi/2)} \tag{8.11}$$

and thus, with $\psi = -2\Delta k(x - U\Delta r)$,

$$h_1(U, x) = e^{-2ju_1\Delta k(x - U\Delta r)} e^{-j(N-1)\Delta k(x - U\Delta r)} \frac{\sin[N\Delta k(x - U\Delta r)]}{\sin[\Delta k(x - U\Delta r)]} \tag{8.12}$$

As $N \to \infty$, $|h_1(U, x)|^2$ becomes (for a given scatterer location x) a sinc-squared function of U with the usual −13.3 dB sidelobes. Note that, if the scatterer lies exactly on the pixel location U, then at the peak of the PSF ($x = U\Delta r$), the phase is zero, independent of U. The processing is such that, for each pixel, the peak of the PSF for a scatterer at that exact pixel location will have zero phase.

The pixel phase is given by

$$\Phi(U, x) = -2\left(u_1 + \frac{N-1}{2}\right)\Delta k(x - U\Delta r) = -2\overline{k}(x - U\Delta r) \quad (8.13)$$

Thus, for fixed U, $\delta\Phi = -2\overline{k}\delta x$, where $\overline{k}$ is the average wavenumber. That justifies (at least for one-dimensional images) the statement made in Section 7.5.3.4 concerning IFSAR that, for a given pixel of an image of a single point scatterer, if the scatterer is shifted by a small distance from one image to another, the pixel phase change is the same as for a monochromatic wave at the average transmitted frequency.

As discussed in Section 7.3.1, the signal data can be multiplied by a weighting function prior to the DFT/FFT, resulting in increased mainlobe width and reduced sidelobe levels.

8.1.6 Range Window

We want to form our downrange image over a window of length L; thus, $\Delta r = L/N$. It is useful to choose $\Delta k = \pi/L$, so that $\Delta k\Delta r = \pi/N$, $\Delta f = c\Delta k/2\pi = c/2L$, $L = c/2\Delta f$, and $\Delta r = c/2N\Delta f \cong c/2B$. Then, from (8.10),

$$h_1(U, x) = e^{-2j\Delta k u_1(x - U\Delta r)} \sum_{u=0}^{N-1} e^{-2\pi jux/L} e^{2\pi juU/N} \quad (8.14)$$

From (8.3b), substituting $k \to U$, $n \to u$, $g(kT) \to h_1(U)$ and $G(n/NT) \to e^{-2\pi jux/L}$ we see that (8.14) is equivalent to performing a DFT (FFT) on the discrete set of complex signal samples. The peak-to-first-null downrange resolution is $\delta_{rpn} = \Delta r = c/2B$.

We set $x \equiv R + r$, where R is the distance to the near edge of the window of length L, and $0 < r < L$. In general, R is many times the size of L. Then, from (8.14),

$$h_1(U, R, r) = e^{-2j\Delta k u_1(R + r - U\Delta r)} \sum_{u=0}^{N-1} e^{-2\pi juR/L} e^{-2\pi jur/L} e^{2\pi juU/N} \quad (8.15)$$

We set $R = (M + \alpha)L$, with M an integer and $0 < \alpha < 1$. Then

$$h_1(M, \alpha, U, r) = e^{-2\pi j u_1 M} e^{-2\pi j u_1 [\alpha + (r - U\Delta r)/L]} \sum_{u=0}^{N-1} e^{-2\pi j u M} e^{-2\pi j u \left(\alpha + \frac{r}{L} - \frac{U}{N}\right)} \tag{8.16}$$

Because u, u_1, and M are integers, the first factor and the first factor after the sum are each equal to unity. Thus, the image of each scatterer (and, more generally, the image of the scene) is independent of M and depends only on the position of the scatterer in the window, not on the absolute distance from the window to the radar (assuming no significant variation in R^4, or other complication, such as multipath).

This concept is illustrated in Figure 8.4. We may consider the radar located at the first of a series of points in space separated by a distance L (the author refers to those points as "fence posts"). For a radar on the ground with pulse width τ illuminating the ground, the swath width of the observed scene resulting from each signal sample will be $c\tau/2$ (Section 1.17). Figure 8.5 illustrates various relationships between the image window and the observed swath.

We now assume downconversion to baseband, specifically $u_1 = 0$, and $\alpha = 0$. Then

$$h_1(U, r) = \sum_{u=0}^{N-1} e^{-2\pi j u \left(\frac{r}{L} - \frac{U}{N}\right)} \tag{8.17}$$

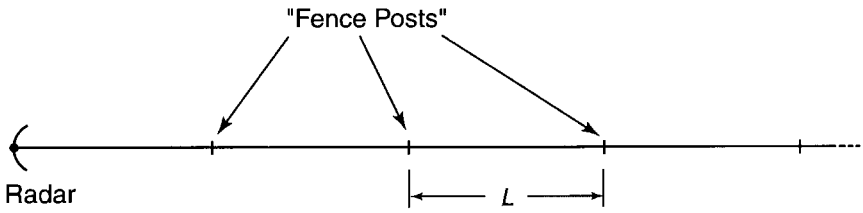

Δf = frequency increment

L = range window = $\frac{c}{2\Delta f}$

N = number of frequencies

$\Delta r = \frac{L}{N-1} = \frac{c}{2(N-1)\Delta f} = \frac{c}{2B}$

Figure 8.4 Range windows.

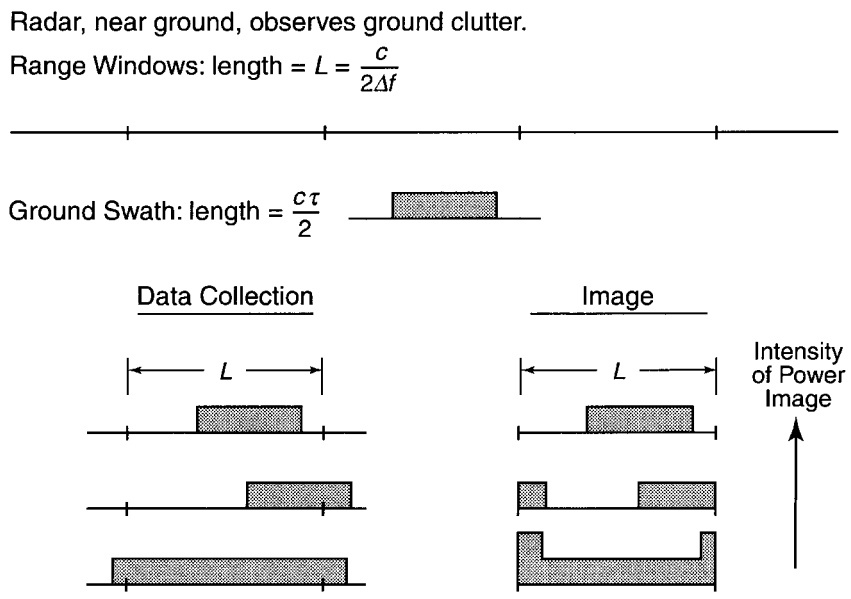

Figure 8.5 Relationship between range windows and pulse width.

From (8.11), the phase of that quantity is

$$\Phi(U, r) = -(N-1)\pi\left(\frac{r}{L} - \frac{U}{N}\right) \tag{8.18}$$

For fixed r,

$$\left(\frac{\delta\Phi}{\delta U}\right)_r = \left(\frac{N-1}{N}\right)\pi \tag{8.19}$$

Thus, for large N, the phase change between adjacent pixels is approximately π. For $r = 0$,

$$\Phi(U, 0) = \pi U\left(\frac{N-1}{N}\right) \tag{8.20}$$

Table 8.1 illustrates examples of pixel phase for some simple cases.

Table 8.1
Pixel Phase

$$|\Phi(U, 0)| = \pi U\left(\frac{N-1}{N}\right) \tag{8.20}$$

$N = 8$:									
U:	0	1	2	3	4	5	6	7	"8"
$\lvert\Phi/\pi\rvert$	0	7/8	14/8	21/8	28/8	35/8	42/8	49/8	7
$\lvert\Phi/\pi\rvert$ mod 2	0	7/8	14/8	5/8	12/8	3/8	10/8	1/8	1
$N = 7$:									
U:	0	1	2	3	4	5	6	"7"	
$\lvert\Phi/\pi\rvert$	0	6/7	12/7	18/7	24/7	30/7	36/7	6	
$\lvert\Phi/\pi\rvert$ mod 2	0	6/7	12/7	4/7	10/7	2/7	8/7	0	

If the sequence of pixels is extended to $U = N$, then $|\Phi(N)|$ mod $2\pi = \pi$ for N even, 0 for N odd.

8.2 Digital Image Enhancement (Image Processing)

We now assume that we have an unweighted SAR/ISAR complex image processed with uniform (i.e., no) weighting, with each point scatterer represented by a sinc PSF. We investigate ways of reducing the mainlobe width and reducing the sidelobes of those PSFs.

We introduce the following definitions.

- *Mainlobe narrowing* is a processing procedure that narrows mainlobes.
- *Sidelobe reduction* is a processing procedure that reduces sidelobes.
- *Resolution* is the minimum distance between two point targets such that they can be individually resolved (observed) in the image. A resolution criterion must be stated. A simple criterion is the Rayleigh criterion [3, p. 8–28], which states simply that the resolution is equal to Δr. A more sophisticated criterion could invoke the discussion of Section 4.3 and would depend on the SNR and the PSF shapes, including sidelobe levels.
- *Superresolution* is a processing procedure that improves resolution beyond the limits of the DFT.

Mainlobe narrowing and superresolution are not necessarily the same thing.

8.2.1 Introduction to Superresolution and Sidelobe Reduction Techniques

DeGraaf [4] has produced a useful review of the aforementioned image enhancement techniques. Except as noted, the remainder of this chapter follows [4]. The techniques are collectively known as spectral estimation techniques, reflecting the fact that the processing implicitly makes an estimate of portions of the input signal not explicitly present, to obtain an improved output, that is, a narrowed mainlobe and/or reduced sidelobes for point scatterers.

Following DeGraaf, we define $\mathbf{X}$ as a column vector containing the radar signal history samples. For a two-dimensional image consisting of p_x by p_y pixels, we use a $p_x p_y$ by 1 column vector. We assume that resampling from any focusing algorithm (PFA, RMA, etc.) has already occurred, so that, for conventional signal processing, only a two-dimensional weighted DFT remains to be performed.

We also introduce the expected value of a signal or image parameter a, denoted by $\mathrm{E}(a)$. The expected value refers to the average value of the parameter that would be obtained if the data collection were performed many times under nominally (but not exactly) identical conditions (an ensemble of data collections). If that were actually done, the specific measured values of noise and clutter voltages would vary from collection to collection; if desired, the variations could be modeled according to a probability density function (see Section 4.1.2). $\mathrm{E}(a)$ can be regarded as a theoretical ideal. More practically, it can be estimated, for example, by averaging a over an entire signal history, then (1) processing assuming that the average is the expected value, or (2) processing only a portion of the signal history but using $\mathrm{E}(a)$ as estimated from the entire history.

Using $\mathrm{E}(a)$, we define the signal history covariance matrix:

$$\begin{aligned} \mathbf{R} &= E(\mathbf{X}\mathbf{X}^{\mathbf{H}}) \\ R_{ij} &= E(x_i x_j^*) \end{aligned} \tag{8.21}$$

Here the superscripted variable $\mathbf{X}^{\mathbf{H}}$ refers to the Hermitian adjoint, or conjugate transpose [5], of the matrix (vector) $\mathbf{X}$; x_i refers to the ith component of $\mathbf{X}$; and * represents complex conjugation. For the diagonal elements of $\mathbf{R}$, $i = j$ and

$$R_{ij} = E(x_i x_i^*) = E(|x_i|^2) \tag{8.22}$$

Because measured voltages may be either positive or negative, we assume x_i is a zero-mean variable; $\mathrm{E}(|x_i|^2)$ is its variance. More generally, $E(x_i x_j^*)$ is the covariance between x_i and x_j; hence, the nomenclature.

8.2.2 DFT (FFT) Processing

Let us consider data resulting from illuminating a point target at range r with a waveform utilizing N frequencies separated by Δf, with echo signals downconverted to baseband. The transmitted wavenumbers (minus the carrier) are $k_n = n\Delta f$, $n = 0, 1, \ldots, N-1$. From (8.6), the echo complex samples are

$$W(n, r) = e^{-2jnr\Delta k} \tag{8.23}$$

which may be represented by a column vector $\mathbf{W}(r)$. We define $\mathbf{x}$ as the image (again a column vector containing all pixels, perhaps usually displayed in two dimensions). The image resulting from processing with an unweighted DFT then can simply be expressed as (Problem 8.2)

$$\mathbf{x}(\mathbf{r}) = \mathbf{W}^{\mathbf{H}}(\mathbf{r})\mathbf{X} \tag{8.24}$$

A weighted DFT image may be written

$$\mathbf{x}(\mathbf{r}) = \mathbf{W}^{\mathbf{H}}(\mathbf{r})\mathbf{A}\mathbf{X} \tag{8.25}$$

where $\mathbf{A}$ is a real-valued diagonal matrix corresponding to a weighting function. To quote from [4, p.733]:

> Unweighted FFT image formation corresponds to evaluating a bank of matched filter outputs, each filter being matched to a point target at a particular spatial location. In the simple case of a single point target in white Gaussian noise or clutter, this matched filter maximizes SIR [signal-to-interference ratio].

For the simple case of a scene containing a single point target exactly on a pixel location r_0,

$$\begin{aligned} \mathbf{X} &= \mathbf{W}(\mathbf{r_0}) \\ \mathbf{x}(\mathbf{r}) &= \mathbf{W}^{\mathbf{H}}(\mathbf{r})\mathbf{W}(\mathbf{r_0}) = \delta_{rr_0} \end{aligned} \tag{8.26}$$

(Problem 8.3). Here δ_{ab} is the Kronecker delta [6]; $\delta_{ab} = 1$ if $a = b$, $\delta_{ab} = 0$ if $a \neq b$, where a and b are integers.

8.2.3 Periodogram

A simple extension of the weighted DFT is the periodogram, which is the expected value of the power image over an ensemble of data collections. Thus,

$$\begin{aligned}\mathbf{x}(\mathbf{r}) &= \mathbf{E}(|\mathbf{W}^{\mathbf{H}}\mathbf{A}\mathbf{X}|^2) = \mathbf{E}(\mathbf{W}^{\mathbf{H}}\mathbf{A}\mathbf{X}\mathbf{X}^{\mathbf{H}}\mathbf{A}\mathbf{W}) \\ &= \mathbf{W}^{\mathbf{H}}\mathbf{A}\mathbf{E}(\mathbf{X}\mathbf{X}^{\mathbf{H}})\mathbf{A}\mathbf{W} = \mathbf{W}^{\mathbf{H}}\mathbf{A}\mathbf{R}\mathbf{A}\mathbf{W}\end{aligned} \tag{8.27}$$

However, to improve on a weighted DFT, a periodogram requires an independent estimate of **R**, which generally is not available.

To appreciate one application of a periodogram, recall the concept of *speckle* in a SAR image (Section 7.3.5). Many SAR images of clutter exhibit pixel-to-pixel intensity fluctuations greater than are seen in comparable optical images. That phenomenon, known as speckle, occurs because, in ground clutter (notably vegetation), although neighboring pixels may have similar numbers of scatterers, each with similar values of radar cross-section, the overall magnitudes of the pixels may vary substantially because of differences in the detailed manner by which the scatterer phases add together. Speckle is usually considered undesirable, and one way to reduce it is for the SAR, as it passes each region of the scene, to "look" several times at each region, forming a SAR image for each look. The images are then averaged noncoherently, a procedure known as multilook.

A generalization of the multilook procedure is to collect data over a particular aperture (the "full" aperture) and compute **R** for the full aperture, then form a periodogram image over a subaperture using **R** as determined for the full aperture. However, that results in reduced crossrange resolution. According to [4], "for this reason, the periodogram is of little practical interest."

8.2.4 Minimum-Variance Method

The minimum-variance method (MVM) is also known as the maximum-likelihood method and Capon's method. For a point target at a particular pixel location, it is a theoretically ideal procedure for maximizing the energy in the correct pixel (mainlobe) and minimizing the energy outside it (sidelobes).

The most general linear procedure for determining the pixel value $\mathbf{x}(\mathbf{r})$ at the target location $\mathbf{r}$ is

$$\mathbf{x}(\mathbf{r}) = \mathbf{A}^{\mathbf{H}}(\mathbf{r})\mathbf{X} \tag{8.28}$$

We want to find the optimum $\mathbf{A}(\mathbf{r})$. We impose the constraint that

$$\mathbf{A}^{\mathbf{H}}(\mathbf{r})\mathbf{W}(\mathbf{r}) = 1 \tag{8.29}$$

to ensure that the point target signal passes the filter with unit (i.e., maximum) gain. We then minimize

$$E(|\mathbf{x}(\mathbf{r})|^2) = E(|\mathbf{A}^{\mathbf{H}}\mathbf{X}|^2) = \mathbf{A}^{\mathbf{H}}\mathbf{R}\mathbf{A} \tag{8.30}$$

to minimize the sidelobes. It can be shown [4 and references therein] that

$$\mathbf{A} = \frac{\mathbf{R}^{-1}\mathbf{W}}{\mathbf{W}^{\mathbf{H}}\mathbf{R}^{-1}\mathbf{W}} \tag{8.31}$$

(see also Section 9.2). The numerator is a vector and the denominator is a scalar. Therefore,

$$\mathbf{x}(\mathbf{r}) = \mathbf{A}^{\mathbf{H}}\mathbf{X} = \frac{\mathbf{W}^{\mathbf{H}}\mathbf{R}^{-1}\mathbf{X}}{\mathbf{W}^{\mathbf{H}}\mathbf{R}^{-1}\mathbf{W}} \tag{8.32}$$

Determining $\mathbf{R}$ requires an estimate of the ensemble of data collections. Computing $\mathbf{R}^{-1}$ dominates the computational complexity. A typical two-dimensional SAR spot image may have several thousand pixels on a side; thus, the column vector $\mathbf{A}$ may have several million rows, and the square matrix $\mathbf{R}$ may have over a trillion elements. Current research focuses on methods for reducing the level of computational complexity while preserving the basic advantages of the procedure.

8.2.5 High-Definition Vector Imaging

Benitz [7] has developed a procedure, referred to as high-definition vector imaging (HDVI), for working with a covariance matrix that has reduced rank relative to the $\mathbf{R}$ matrix referred to above (the rank of a matrix is the number of independent rows [5]). (DeGraaf calls the technique the "reduced-rank minimum-variance method.") The weighting coefficients $\mathbf{W}$ are constrained in a manner described in [6], resulting in reduced computational requirements relative to the MVM.

Of particular interest is the vector aspect of HDVI. A series of matched filters is applied to the phase history data, each tuned for a different elementary target type, including the point scatterer, flat plate, dihedral, trihedral, and cylinder on a ground plane. HDVI then processes the image according to each

matched filter. The output is an image with each pixel represented by a multicomponent vector, which then can be further compared with the expected target type. Figure 8.6 illustrates the principle of HDVI, and Figure 8.7 shows some illustrative results.

8.2.6 Adaptive Sidelobe Reduction

DeGraaf [4] has developed a still simpler approximation to the MVM, which is referred to as adaptive sidelobe reduction (ASR). Although the method can easily be used for two-dimensional data and imagery, to illustrate it we discuss the simpler one-dimensional case. Thus, **r** becomes r. With complete generality, we can write

$$x(r) = \mathbf{A}^{\mathbf{H}}\mathbf{X} = \sum_{k=0}^{K-1} A_k(r) X_k e^{2\pi jrk/N} \tag{8.33}$$

Simplicity is achieved by requiring that the A_k be real. If they were constant and independent of the pixel, that is, if $A_k(r) = A_k$, the procedure would be a weighted DFT interpolated by a zero-padding factor $R = N/K$. ASR is more general than the weighted DFT because the weighting coefficients are dependent on the pixel value; hence, the term *adaptive*.

We now set

$$A_k(r) = 1 + \sum_{m=1}^{M} a(r, m)\cos(2\pi mk/K),\ M \ll K \tag{8.34}$$

That is actually similar to Taylor weighting [1, Sec. D.2], except that for Taylor weighting the $a(r, m)$ becomes $a(m)$, independent of the pixel. We require that R be an integer. Then, substituting (8.34) into (8.33), we find (Problem 8.4)

$$x(r) = y(r) + \sum_{m=1}^{M} \frac{a(r, m)}{2}[y(r - Rm) + y(r + Rm)] \tag{8.35}$$

where $y(r)$ is the unweighted DFT image for which a point target is represented by a sinc function.

Equation (8.35) is in the form of a convolution, reflecting the fact that multiplication in the signal domain (8.33) yields convolution in the image domain. If $R = 1$, the convolution utilizes the M nearest pixels on each side of the pixel being computed. If $R > 1$, then every Rth pixel is used. In either

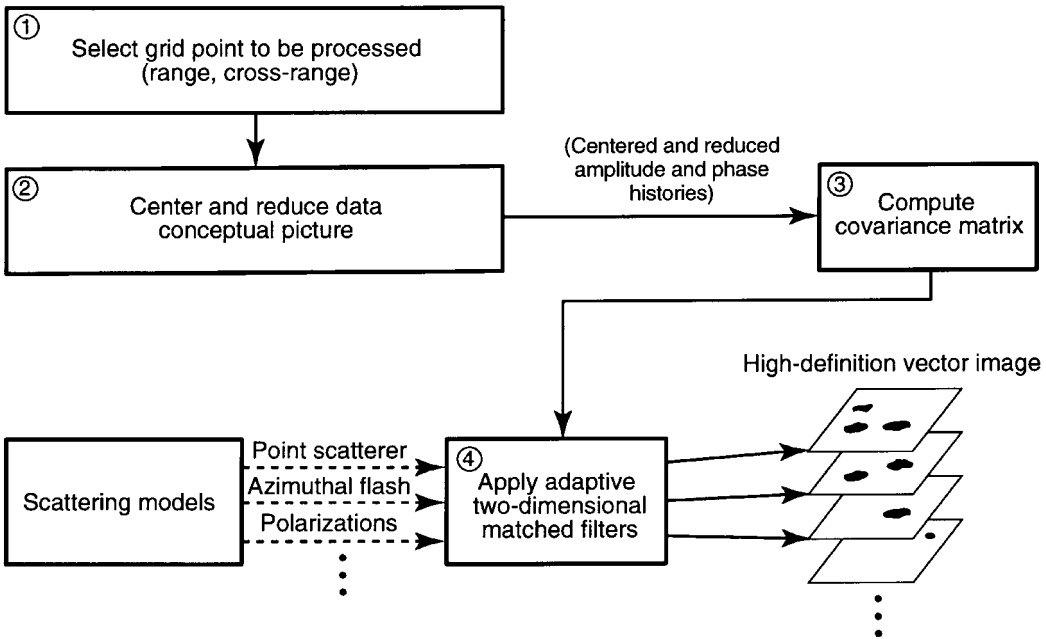

The processing flow in HDVI. The image is processed in small image chips, and a covariance matrix is formed for each chip. The adaptive-filtering technique (e.g., Capon's technique) employs the covariance matrix and the desired scattering model to produce the high-definition vector image.

Figure 8.6 Principles of HDVI. (After [6], with permission of MIT Lincoln Laboratory, Lexington, MA.)

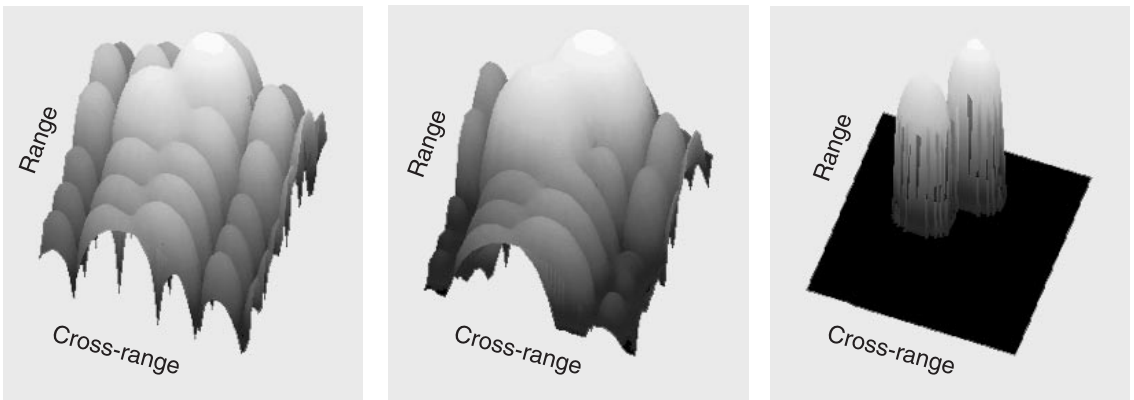

Figure 8.7 HDVI results. (Reproduced from [6], with permission of MIT Lincoln Laboratory, Lexington, MA.)

case, $2M$ pixels are used to compute the convolution. ASR thus can be performed by first generating the unweighted DFT image, then performing a convolution on the complex pixel values.

DeGraaf [4] presents an example of an ASR-processed image with an "order" (M) of 2. Computation of the coefficients $a(r, m)$ is explained in [4].

For a two-dimensional image, we can apply ASR successively to rows and columns (the separable method) or utilize a two-dimensional generalization of (8.34) as follows:

$$A(n_x, n_y, k_x, k_y) = 1 + \sum_{m_x=0}^{M} \sum_{m_y=0}^{M} a(n_x, n_y, m_x, m_y) \cos\left(\frac{2\pi m_x k_x}{K_x}\right) \cos\left(\frac{2\pi m_y k_y}{K_y}\right) \tag{8.36}$$

The sum does not include the term $m_x = m_y = 0$.

8.2.7 Spatially Variant Apodization

Stankwitz et al. [8] (also discussed in [1, Sec. D.3]) have developed a simple form of ASR called spatially variant apodization (SVA). *Apodization*, a term originally coined to refer to sidelobe reduction in optical systems, comes from the Greek α, *take away*, and $\pi o \delta o \varsigma$, *foot*, meaning literally *removing the feet from* [9, 10]. SVA is simply ASR with $M = 1$, $R = 1$, and $a(r) > 0$. Specifically

$$\begin{aligned} A_k(r) &= 1 + a(r)\cos(2\pi k/K) \\ x(r) &= \sum_{k=0}^{K-1} A_k(r) X_k e^{2\pi jrk/K} \\ x(r) &= y(r) + \frac{a(r)}{2}(y(r-1) + y(r+1)) \end{aligned} \tag{8.37}$$

SVA involves a convolution of the unweighted FFT complex image using only the nearest neighbors of each pixel. That simplicity means very little computational burden. Although SVA is efficient at lowering sidelobes, it cannot reduce mainlobe width. Again, the procedure for calculating the $a(r)$ is given in [8].

8.2.8 Super-SVA

Super-SVA, also developed by Stankwitz et al. [11], is a bandwidth-extrapolation procedure that has been found experimentally to reduce the mainlobe

width, lower the sidelobes, and produce "pleasing" SAR imagery. As shown in Figure 8.8, the procedure is as follows:

1. Begin with unweighted data in the signal domain.
2. Produce an unweighted FFT image.
3. Perform SVA (or complex dual apodization [1]).
4. Perform an inverse FFT; multiply by an inverse weighting function, which produces extrapolated signal data of essentially constant amplitude over a wider bandwidth than the original data and truncates the signal data beyond the point where it has significant amplitude.
5. Replace the central portion of the modified signal data with the original signal data.
6. Again produce an unweighted FFT image.
7. Again perform SVA, and so on.

The procedure can be iterated.

Stankwitz and Kosek [12] have also shown that super-SVA can be used to interpolate over gaps in the bandwidth of a received signal. Such gaps could result from, for example, legal restrictions on the transmitted signal or the necessity to discard some portion of the received signal due to interference in a particular frequency window. They present examples of simulated imagery obtained both with the original, nongapped received signal and with the gapped received signal using super-SVA.

8.2.9 Other Spectral Estimation Techniques and Applications

Many other spectral estimation techniques for improving imagery are discussed in the literature and summarized in [4]. Some of these include the following:

- Autoregressive linear prediction (ARLP);
- Pisarenko's method;
- Eigenvector (EV) and multiple signal classification (MUSIC);
- Tufts-Kumaresan ARLP; and
- Parametric maximum likelihood (PML).

Furthermore, by increasing matrix dimensions, some spectral estimation techniques can be extended to include

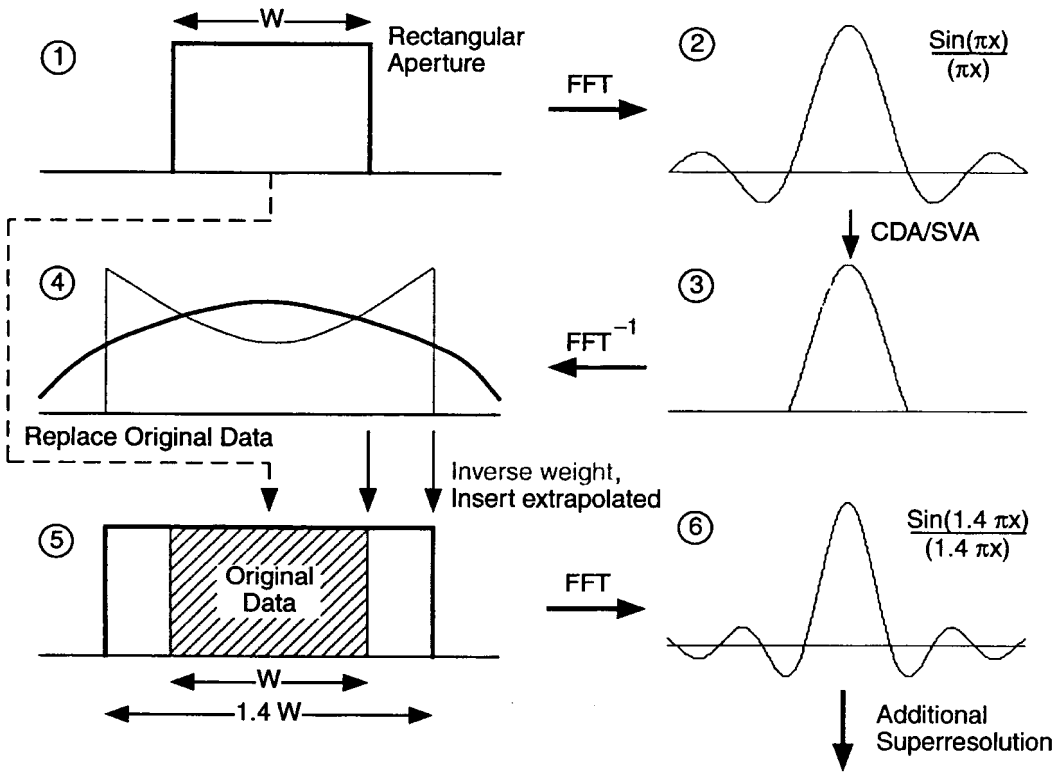

Figure 8.8 Super-SVA. (Courtesy of Veridian ERIM-International.)

- IFSAR, thereby improving vertical, as well as horizontal, resolution;
- Polarimetric SAR imagery with two to four channels representing different combinations of polarizations, for example, HH (transmit H, receive H), HV, VH, and VV, or their circular-polarization analogs.

8.2.10 Example Results

Figure 8.9 compares PSFs for a number of spectral estimation algorithms. The data are from an actual SAR image of a trihedral corner reflector on an asphalt causeway. The top portion of the figure summarizes results of the "easy" methods, that is, those methods that do not involve extensive computation: sinc, Taylor, SVA, ASR, and super-SVA. Regarding the mainlobe, Taylor is widest, sinc and SVA are the same, and second widest, ASR is third widest, and super-SVA is narrowest. Sinc, of course, has the highest sidelobes; the Taylor sidelobes are quite regular and generally second highest; the sidelobes

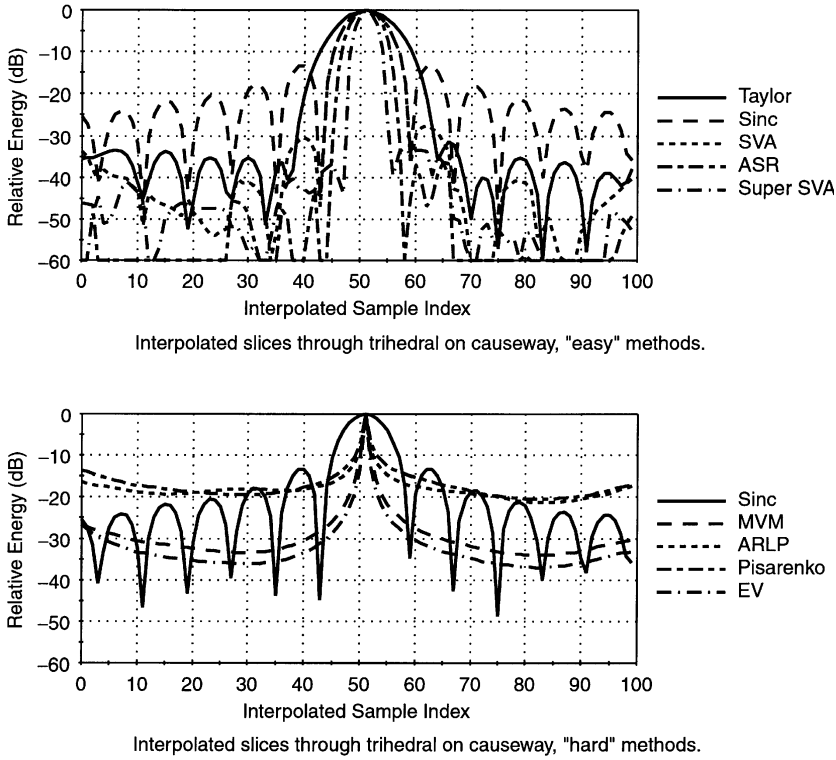

Figure 8.9 PSFs for spectral estimation techniques. (Reproduced from [4], Figures 17 and 18, copyright 1998, IEEE.)

of the other methods are lower and quite irregular. The bottom portion of the figure shows the results of several "hard" methods, compared with sinc. All have mainlobes much narrower than those previously discussed. ARLP and Pisarenko have relatively high sidelobes; MVM and EV have lower and very smooth sidelobes.

DeGraaf [4] presents images of the same simulated scene, with target-to-clutter ratio of 13 dB, processed via many different algorithms. He also includes six actual SAR images of two ships at a dock near Toledo, Ohio, processed according to different algorithms, and provides a detailed discussion of those results.

8.2.11 Comment on Spectral Estimation Techniques

As the name implies, spectral estimation involves estimating signal data. In most cases of interest, such estimation may be justified, but there may be pathological cases where it is not. The user should be appropriately cautious, especially where fine details of images are concerned.

References

[1] Carrara, W. G., R. S. Goodman, and R. M. Majewski, *Spotlight Synthetic Aperture Radar*, Norwood, MA: Artech House, 1995.

[2] Brigham, E. O., *The Fast Fourier Transform and Its Applications*, Englewood Cliffs, NJ: Prentice Hall, 1988.

[3] Wolfe, W. L., and G. Zissis (eds.), *The Infrared Handbook*, rev. ed, Ann Arbor, MI: Environmental Research Institute of Michigan, 1989.

[4] DeGraaf, S. R., "SAR Imaging via Modern 2-D Spectral Estimation Methods," *IEEE Trans. Image Processing*, Vol. 7, No. 5, May 1998, pp. 729–761.

[5] Strang, G., *Linear Algebra and Its Applications*, 3rd ed., San Diego: Harcourt Brace Jovanovich, 1988.

[6] Korn, G. A., and T. M. Korn, *Mathematical Handbook for Scientists and Engineers*, New York: McGraw-Hill, 1961.

[7] Benitz, G. R., "High-Definition Vector Imaging," *Lincoln Laboratory J.*, Vol. 10, No. 7 (Special issue on Superresolution), 1997, pp. 147–170.

[8] Stankwitz, H. C., R. J. Dallaire, and J. R. Fienup, "Non-Linear Apodization for Sidelobe Control in SAR Imagery," *IEEE Trans. Aerospace and Electronic Systems*, Vol. 31, No. 1, Jan. 1995, pp. 267–279.

[9] Hecht, E., and A. Zajac, *Optics*, Reading, MA: Addison-Wesley, 1979.

[10] Jacquinot, P., and B. Roizen-Dossier, "Apodization," in E. Wolf (ed.), *Progress in Optics*, Vol. 3, Amsterdam: North-Holland, 1964, p. 29.

[11] Stankwitz, H. C., and M. R. Kosek, "Super-Resolution for SAR/ISAR RCS Measurement Using Spatially Variant Apodization (Super-SVA)," *Proc. Antenna Measurement and Techniques Association (AMTA) Symp.*, Williamsburg, VA, Nov. 1995.

[12] Stankwitz, H. C., and M. R. Kosek, "Sparse-Aperture Fill for SAR Using Super-SVA," *Proc. 1996 IEEE National Radar Conference*, Ann Arbor, MI, 1996, pp. 70–75.

Problems

Problem 8.1

a. Using a computer, verify the principle shown in Figure 8.1, that is, choose a function in the signal domain, compute the $|\text{FFT}|^2$ in the image domain, and verify that adding $M/2$ zeroes before and after the signal results in a more finely sampled version of the image domain function.

b. Revise the equations in Figure 8.1 to make them appropriate for the case where N is odd.

Problem 8.2

Verify (8.24), that is, for a one-dimensional image, $\mathbf{x}(r) = \mathbf{W}^{\mathbf{H}}(r)\mathbf{X}$ corresponds to performing an FFT on the signal data $\mathbf{X}$. (Note: This extends to two- and three-dimensional images.)

Problem 8.3

Verify (8.26), that is, for an unweighted, unpadded one-dimensional image of a point target that lies exactly on a pixel location, the image value is zero for all other pixel locations.

Problem 8.4

Verify (8.35) by substituting (8.34) into (8.33), that is, one-dimensional ASR can be performed by first forming an unweighted image, then modifying each pixel by computing a complex correction factor that is a function of M pixels on each side.